Stability and performance of $CsPbI_2Br$ thin films and solar cell devices

Authors

Silvia Mariotti[1]*, Oliver S. Hutter[1], Laurie J. Phillips[1], Peter J. Yates[1], Biswajit Kundu[2], Ken Durose[1].

Affiliation: 1. Stephenson Institute for Renewable Energy / Department of Physics, University of Liverpool, Liverpool, L69 7ZF, United Kingdom.

2. Department of Solid State Physics, Indian Association for the Cultivation of Science, Jadavpur, Kolkata 700032, India

**E-mail: silvia.mariotti@liverpool.ac.uk*

Keywords

Perovskites, caesium perovskites, inorganic perovskites, stability, solar cells, photovoltaics.

Abstract

In this manuscript the inorganic perovskite $CsPbI_2Br$ is investigated as a photovoltaic material that offers higher stability than the organic-inorganic hybrid perovskite materials. It is demonstrated that $CsPbI_2Br$ does not irreversibly degrade to its component salts as in the case of methylammonium lead iodide, but instead is induced (by water vapour) to transform from its metastable brown cubic (1.92 eV band gap) phase to a yellow phase having a higher band gap (2.85 eV). This is easily reversed by heating to 350°C in a dry environment. Similarly, exposure of un-encapsulated photovoltaic devices to water vapour causes current (J_{SC}) loss as the absorber transforms to its more transparent (yellow) form, but this is also reversible by moderate heating, with over 100% recovery of the original device performance. NMR and thermal analysis show that the high band gap yellow phase does not contain detectable levels of water, implying that water induces the transformation, but is not incorporated as a major component. Performances of devices with best efficiencies of 9.08% (V_{OC} = 1.05 V, J_{SC} = 12.7 $mA.cm^{-2}$ and *FF* = 68.4%) using a device structure comprising glass/ITO/c-TiO_2/$CsPbI_2Br$/Spiro-OMeTAD/Au are presented and further results demonstrating the dependence of the performance on the preparation temperature of the solution processed $CsPbI_2Br$ films are shown. We conclude that encapsulation of $CsPbI_2Br$ to exclude water vapour should be sufficient to stabilise the cubic brown phase, making the material of interest for use in practical PV devices.

Introduction

In the past few years, more stable alternatives have been sought to improve upon the highly efficient but unstable 'hybrid perovskite' class of solar energy materials. The first material from the parent group to be used for photovoltaics, methylammonium lead iodide ($CH_3NH_3PbI_3$ –'MAPI'), exemplifies the problems: it is degraded to its component salts by water,[1–4] or else by a combination of UV-radiation and oxygen which promotes a radical reaction.[5–8] It is also thermally unstable close to its working temperature and the devices are prone to hysteresis.[9,10] In the past few years some groups have tried simple substitution of the halide[11] or the organic cations,[12–14] and passivation[15] but these methods did not solve the stability issues. However it has been recently proven that using mixed perovskite compositions,[16] surface passivation or interface engineering[17,18] and chemical doping[19] can help improve the perovskite's device stability.[4,20–22]

Alternatively, wholly inorganic perovskite analogues are proposed as offering a combination of high performance and enhanced stability. In particular, the mixed halide perovskites $ABX_{3-x}Y_x$ offer further tunability of their electrostatic stability and band gap – by the substitution of halide ions - for optimum solar performance and practicality.[11,23] Here we demonstrate $CsPbI_2Br$ devices with efficiencies of > 9% and show that the material is vulnerable to fewer environmental factors than hybrid perovskites. Indeed, it does not degrade to its component salts, but its metastable phase (that is used in devices) instead transforms to its more transparent room temperature phase on exposure to water vapour. This transformation is reversible upon heating with no loss of device efficiency. The material was found to be tolerant of a wide range of degradation factors (more than MAPI for example) and $CsPbI_2Br$ is therefore proposed as a more suitable material for use in solar photovoltaic devices, providing it can be suitably encapsulated.

Of the caesium lead halide perovskites, the *single halide* iodine and bromine variants have been investigated,[24,25] but show a combination of desirable and limiting properties. Nevertheless, since both the caesium analogues of iodine and bromine each satisfy the Goldschmidt tolerance factor condition ($0.81 < t < 1.11$),[26] then the full series $CsPbI_{(3-x)}Br_x$ may be exploited to achieve the optimum combination of photon conversion efficiency (band gap value) and of materials stability (from electrostatic considerations).[27,28]

Table 1 shows the reported phases, stability and band gap data for $CsPbI_3$, $CsPbBr_3$ and $CsPbI_2Br$, together with the limited PV device results available on them.[27,29] Sharma *et al.*[25] report a phase diagram for the whole composition range $CsPbI_{(3-x)}Br_x$ and for which all compositions have an orthorhombic – cubic phase transition at a temperature that depends on composition. We now outline further reasons for selecting $CsPbI_2Br$ for

the present study: while $CsPbI_3$ has a black phase (E_g = 1.73 eV) that is in principle suitable for PV devices, it is only stable at T > 310°C and remains metastable at room temperature for just a few minutes,[24,25,30] turning into an insulating, yellow orthorhombic phase[25,28] (showing edge-sharing octahedral chains, as for the NH_4CdCl_3 structure[31,32]). Addition of HI increases this stability to no more than a few hours but this has allowed devices with photon conversion efficiencies of up to 2.9% to be fabricated.[29] Nevertheless, the material is insufficiently stable for PV device use. On the other hand, $CsPbBr_3$ is reported to have an perovskite orthorhombic phase which is stable in air at room temperature,[24] however moderate heating (to 88°C) causes a phase change from orthorhombic to a tetragonal perovskite phase and finally to cubic orange phase (above 130°C).[25,30] Its band gap of 2.25 eV[28] makes it unsuitable for high efficiency single junction devices, however, despite this, devices having photon conversion efficiencies (*PCE*) up to 5.95% have been realised.[33] Hence neither the pure iodide or bromide analogues are ideal for PV devices.

Given these limitations, the mixed halide series $CsPbI_{(3-x)}Br_x$[27,28,34] has begun to be studied to exploit the lower (and therefore more ideal) band gap imparted by the iodine, and the higher electrostatic stability imparted by the smaller ionic radius of bromine. Of this series, $CsPbI_2Br$ has been highlighted and indeed has been shown to be sufficiently *thermally* stable for use in photovoltaic applications.[27,28] However, the reported studies of its stability are limited to an incidental comment[27] that the devices are unstable in ambient air: its stability to other environmental factors such as light, oxygen and water has not been studied prior to this work. Although its band gap is relatively high (1.92 eV), the material is potentially viable for PV, the Shockley – Queisser limit predicting V_{OC} = 1.63 V, J_{SC} = 16.3 mA/cm^2 and efficiencies of up to ~21%.[27,35,36] The large band gap also makes tandem devices with silicon very feasible.[28] To date the highest efficiency reported for single junction $CsPbI_2Br$ solar cells has been 9.8%,[27] but questions remain about its stability to environmental factors other than simple heating.

Material	Room temperature phase	Other phases	PV results	Notes
$CsPbBr_3$	Black orthorhombic phase E_g = 2.25 eV[37] Improper band gap for PV absorber.	T > 88°C Tetragonal phase T > 130°C Orange cubic phase[37]	5.95%[33]	RT phase is stable to degradation but the band gap is too high for a PV absorber.
$CsPbI_2Br$	Brown phase E_g = 1.92 eV Stable in dry ambient.	Yellow phase E_g = 2.85 eV Transformed reversibly from the brown to yellow phase by moisture but does not degrade to its salts (this work).	9.84% champion device[27] 9.08% this work Performance degradation shown to be reversible (this work).	Bromine imparts electrostatic stability while iodine brings the band gap into the useful range for PV applications.
$CsPbI_3$	Yellow orthorhombic phase[29] E_g = 2.85 eV	T > 310°C Black cubic phase	For the metastable black phase: 1.7%,	Black phase has a band gap compatible

	Unsuitable band gap for PV absorber.	E_g = 1.73 eV Metastable at RT for minutes only, HI stabilises it for hours only.[29]	2.9% with HI stabilisation.[29]	with PV, but is not sufficiently stable.

Table 1. Phases, stability, band gaps and device results for the $CsPbI_{(3-x)}Br_x$ series. While the pure iodide compound is unstable, the bromide one has too high a band gap for use as a solar absorber. $CsPbI_2Br$ gains electrostatic stability from the bromide, while the iodide brings the band gap into the useful range for PV applications.

This work presents a systematic study of the fabrication of $CsPbI_2Br$ films and devices, with a best *PCE* of 9.08%. It includes stability trials of both the material and the devices, that demonstrate that the brown perovskite phase (E_g = 1.92 eV) is stable to UV light, oxygen and moderate ozone exposure, but water vapour initiates the phase transformation to a yellow phase (E_g = 2.85 eV). Furthermore, the transformation is reversible by thermal annealing at 350°C in dry conditions. Indeed, PV devices that had been deliberately degraded recover 100% of their performance upon annealing, and sometimes exceeded their original performance. This reversible transformation for $CsPbI_2Br$ contrasts with the case for MAPI which degrades *irreversibly* to its constituent salts i.e. by losing methylammonium iodide, leaving lead iodide.[1,3,5]

Results and discussion

$CsPbI_2Br$ films were fabricated using one-step spin coating and hot plate annealing, as explained in the Supplementary Information. Briefly, solutions of CsI, PbI_2 and $PbBr_2$ in N,N-dimethylformamide/dimethyl sulfoxide (DMF/DMSO) were spun onto ITO/glass substrates and annealed at temperatures between 150 and 350°C, yielding films ~350 nm thick.

Figure 1a-e show the development of the visual appearance, X-ray diffraction patterns (XRD), optical transmission and reflectance, absorption coefficient and Tauc plots for the films with increasing annealing temperature. It was found that temperatures of ≥ 150°C were necessary to form a brown perovskite phase of $CsPbI_2Br$, this being slightly higher than for that used for spin-coated $CsPbBr_3$.[27] However, in order to form completely uniform brown films, higher temperatures were necessary, with 300 - 350°C giving the most crystalline films, as confirmed by the SEM images shown in the Supporting Information (Fig. S1). Films formed at all temperatures had similar XRD patterns (showing preferred orientation peaks at 2θ = 14.6° (100) and 29.6° (200) consistent with those reported in literaure.[27,28] The optical transmission/reflectance behaviour of the films was nearly identical, with E_g being in the range 1.91 – 1.92 eV regardless of the preparation temperature. However, the Tauc plots had insufficient linear portions to reliably estimate the band gap, and so independent confirmation was obtained by the spectroscopic mode scanning probe microscopy (STM) method to investigate the near-edge densities of states. As shown in **Figure 2**, this gave a value of 1.98 eV

which is comparable, if slightly higher than the optical values. Both of these values are comparable to the previously reported value of the optical band gap.[27,28]

Films prepared at all temperatures were taken forward for device making, while only those prepared at 350°C were used in degradation trials, as this yielded the highest device performance.

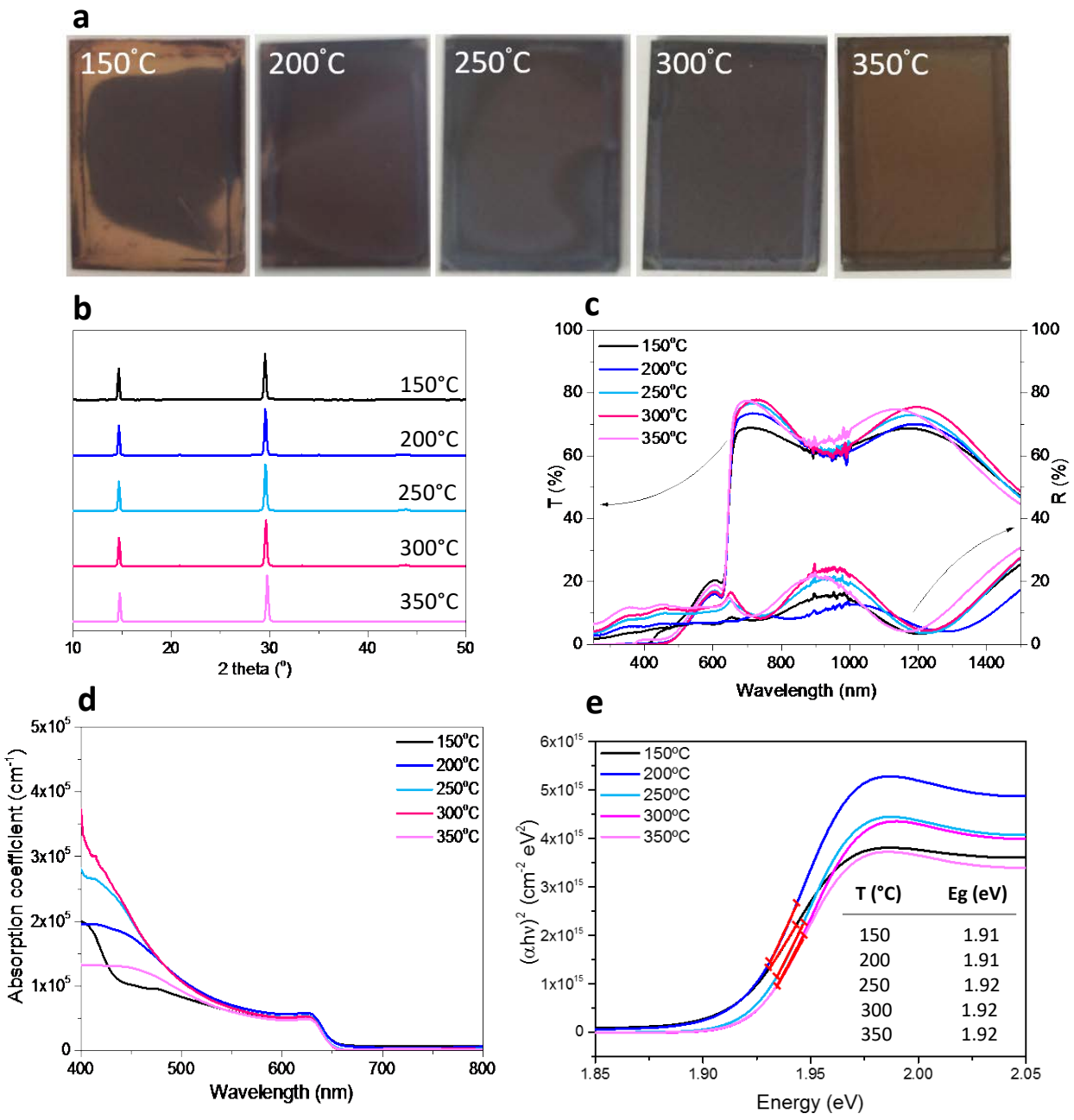

Figure 1. Results of characterisation of $CsPbI_2Br$ films prepared by a one-step process as a function of the annealing temperature: (a) photographs showing the increase in uniformity of the films with temperature (the samples are 20 × 15 mm^2); this statement is supported by SEM images (Supporting Information, Figure S1). (b) XRD demonstrating that the same perovskite phase was achieved for all temperatures $T \geq 150$°C, (c) optical transmission and reflectance spectra used to generate (d) the absorption coefficient behaviour and (e) the Tauc plots for all films showed band gaps in the range 1.91 – 1.92 eV.

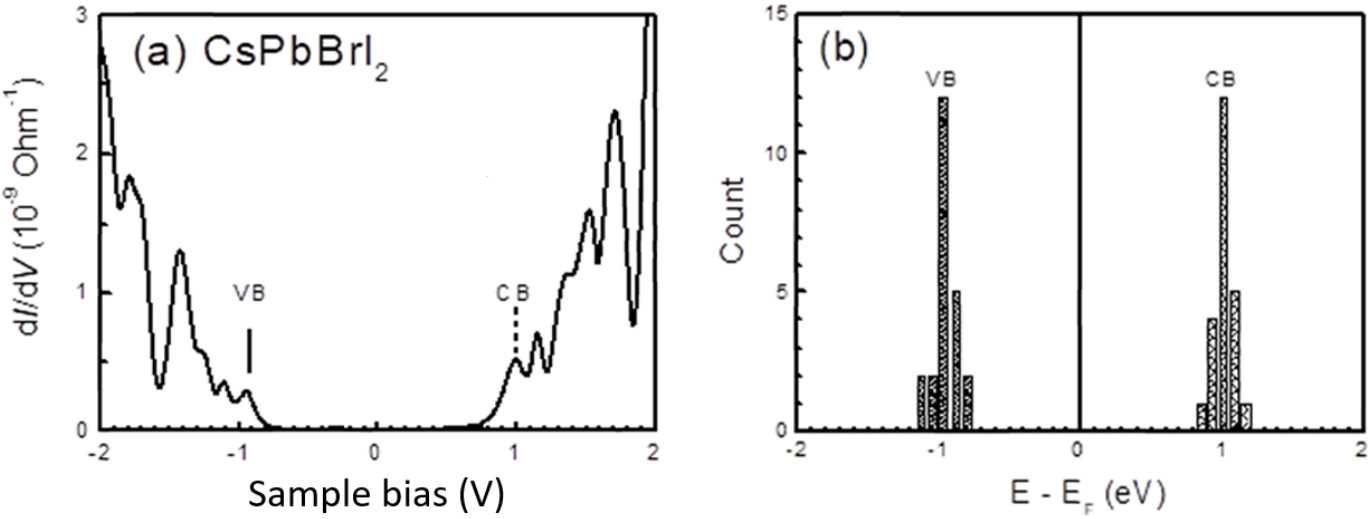

Figure 2. Spectroscopic scanning probe microscopy results for a $CsPbI_2Br$ film prepared at 350°C. The band gap was estimated as 1.98 eV, which is consistent with the values from optical measurements. (a) Shows a typical DOS profile (dI/dV) with the valence and conduction band positions marked. (b) Shows a histogram of the VB and CB positions obtained interrogating 23 separate locations on the sample's surface so as to generate reliable data.

Devices

We have fabricated 'superstrate' configuration PV devices from $CsPbI_2Br$ having the structure shown in **Figure 3**a/b and for which the light passes through the glass and transparent layers before reaching the absorber. As with other perovskite materials, the AM1.5 illuminated *J-V* response (Figure 3c) shows hysteresis, and care was taken to define the performance measurement and stabilisation protocols. The device performances shown in Figure 3c refer to a cell with the structure glass/ITO/TiO_2/$CsPbI_2Br$/Spiro-OMeTAD/Au, where the perovskite film was annealed at 350°C, since this is the annealing temperature that gave the best device performance. We used a voltage scan rate of 0.19 V/s which for the typical device shown in the figure (absorber processed at 350°C) gave a forward scan *PCE* of 6.62% and for reverse 9.08%. This was confirmed by larger data sets: for example, for 16 devices fabricated using material grown at 350°C, the average reverse scan *PCE* was 7.32% while the forward value was 5.34%; however, considering both scans, the average performance of devices with the same film was 6.33%, V_{OC} = 0.9 V, J_{SC} = 11.74 mA/cm^2, *FF* = 60.2%. Figure 3d shows a stabilisation study, i.e. J_{SC} vs time under AM1.5 illumination, for devices made using absorbers fabricated at temperatures in the range 150 - 350°C and having a range of performances. For all devices shown there was a rapid decline in J_{SC} – lasting for between 10 and 30 seconds - before the J_{SC} stabilised, the stabilisation being faster for the higher performing devices. Hence care was taken to measure devices using both forward and reverse scans, and after brief light soaking. Figure 3e and f and **Table 2** show the effects of the $CsPbI_2Br$ preparation temperature on the device performance. Each point in the *PCE* data in Figure 3e and Table 2 is for an average of 16 devices, and shows first a shallow decline

followed by a distinct rise in *PCE* with increasing temperature, above 250°C. A possible explanation for this behaviour may be argued in terms of the conversion of the material from its low to high temperature forms by the annealing during sample preparation, and for which the phase diagram reported by Sharma *et al.*[25] for $CsPbI_xBr_{(1-x)}$ provides insight. In particular, for the composition $CsPbI_2Br$, the phase transition from the orthorhombic (yellow) to the cubic (brown) phase takes place at 195°C, although our DSC study (see later) indicates that it occurs at 255°C. Hence the rise in efficiency above this temperature is expected since the low band gap phase is formed. Furthermore it is likely that the instability of the material at temperatures close to the phase transition gives rise to inferior material and hence the low *PCE* values at 250°C. For annealing temperatures of 150 and 200°C the photographs in Figure 1 show visible macroscopic non-uniformity, with there being orange patches and edge regions several mm in size on the otherwise brown films. Evidently the material has not been uniformly converted to a single phase, and variation in the device performance on the same length scale as the contact dots (2 mm Ø) may be expected. A further factor influencing the device performance is the film morphology, including pinholes and grain size, as shown in the SEM sequence (Figure S1). At 150°C the films have a complex morphology and they appear to be incomplete. At 200°C there is evidence of secondary phases (although EDX of these 300 nm thick layers did not reveal a compositional difference). Hence both of these films had characteristics that would not favour the highest efficiency devices. There is no clear reason why these low temperature devices apparently out-performed those at 250°C, but it should be mentioned that the error bars in Figures 3e and 6b are large, and the effect may be statistical. Finally it is noted that the films prepared at 350°C (highest performing cells) have the most clearly defined and largest grains, these being ~1µm in size (Figure S1). The most dominant performance parameter is *FF* which rises to 60.2% for samples prepared at 350°C – compared to a *FF* of 26.7% at 250°C. Variation of the other performance parameters is less influential, but V_{OC} increases steadily while J_{SC} and *FF* follow the overall trend in efficiency with temperature. For example, the stabilised J_{SC} (Figure 3c) contributes to the efficiency trend with temperature (min at 250°C and max at 350°C), and this is confirmed by the trend in *EQE* responses (Figure 3f).

Overall, the device (0.0314 cm^2 active area) showing the highest efficiency recorded in this work was for material grown at 350°C and yielded V_{OC} = 1.05 V, J_{SC} = 12.68 $mA.cm^{-2}$, *FF* = 68.4% and *PCE* = 9.08%. This is comparable to the highest reported in the literature from Sutton *et al.* with V_{OC} = 1.11 V, J_{SC} = 11.89 $mA.cm^{-2}$, *FF* = 75% and *PCE* = 9.84%.[27] This device result confirms that these studies have been conducted on material that is of quality comparable to that used in the state of the art devices as reported in the international literature.

A description of the *device* degradation is deferred until after our study film stability has been presented in the next section.

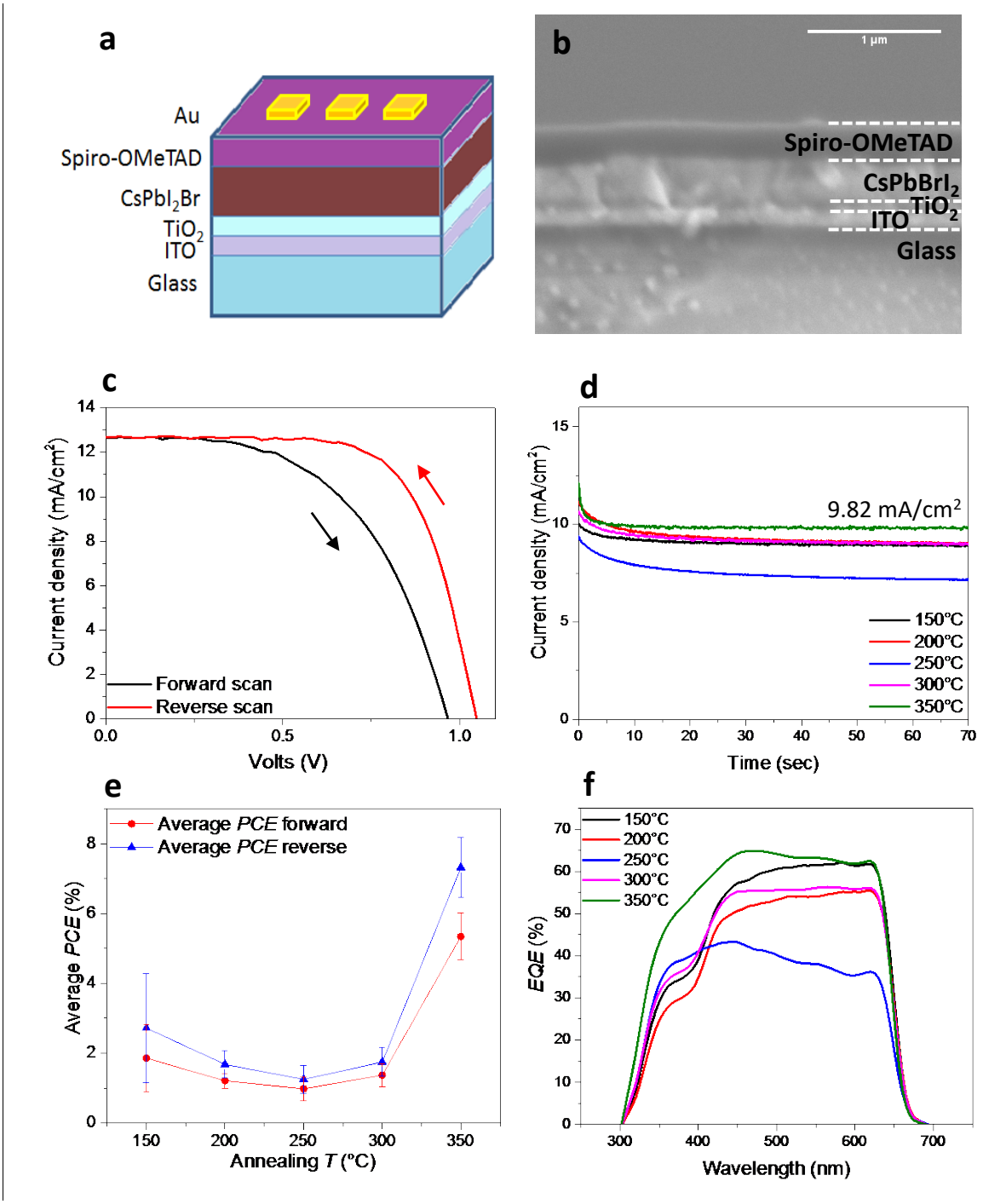

Figure 3. $CsPbI_2Br$ devices with films prepared in the temperature range 150 - 350°C. Figure (a) and (b) show the 'superstrate' design and cross-section SEM of the component layers, (c) shows the hysteretic behaviour of the *J-V* curves for a high performance device; using a scan rate of 0.19 V/s we measured an average reverse scan *PCE* of 9.08% and a forward scan *PCE* of 6.62% – reverse scans gave the highest and most reproducible performing data, (d) the stabilised J_{SC} measured on devices with the perovskite layer annealed at different temperatures showing that the most stable and highest performing devices are annealed at the highest temperature, (e) average *PCE* from forward and reverse scans vs film preparation temperature and (f) the *EQE* (%) confirming that preparation at 350°C yields the highest J_{SC}.

	150°C		200°C		250°C		300°C		350°C	
	As-grown	Aged	As-grown	Aged	As-grown	Aged	As-grown	Aged	As-grown	Aged
V_{OC} (V)	0.67	0.50	0.68	0.51	0.71	0.65	0.73	0.71	0.90	0.79
J_{SC} (mA/cm^2)	9.07	0.16	7.63	0.23	5.83	0.55	7.94	0.26	11.74	0.24
FF (%)	34.8	40.6	28.2	44.5	26.7	42.2	26.9	36.2	60.2	39.7
PCE (%)	2.29	0.03	1.45	0.06	1.11	0.18	1.56	0.07	6.33	0.08

Table 2. Performance parameters for the $CsPbI_2Br$ solar cell devices as a function of the annealing temperature used to prepare the absorber. The data show the averages of forward and reverse scans for 16 devices per data point. The rise in efficiency with temperature is attributed to increase in the J_{SC} and *FF* associated with the increased uniformity of the films. Data for both fresh and aged is shown. Ageing - i.e. exposure to atmospheric water vapour - causes the brown $CsPbI_2Br$ to transform to a more transparent yellow phase, showing a corresponding drop in J_{SC} while V_{OC} remains remarkably high.

Materials stability study

While it is known that $CsPbI_2Br$ is thermally stable, its stability to visible/UV light, water vapour, O_2 and O_3 are not known. Here we investigate the stability of $CsPbI_2Br$ films to these degradation factors. During preliminary handling of $CsPbI_2Br$, it was seen that the films changed from brown to yellow after being removed from the dry glovebox atmosphere, and that the yellow phase had a different XRD signature than the brown perovskite phase $CsPbI_2Br$. Moreover, this new phase did not correspond to the XRD patterns of either the Cs or Pb salts[38] as shown in the Supplementary Information (Figure S5).

Hence a systematic series of experiments was designed to establish the exact causes of this change (see Supplementary Information for details). Briefly they were: 1) UV irradiation under dry nitrogen (two × 9W-L 365nm UV lamps), 2) storage in the dark in air, 3) storage in a desiccator under lab lighting and 4) exposure to UV/O_3 in a cleaner designed for preparing substrates. Tests 1) to 3) were carried out for one week and one month before characterisation by XRD and optical transmission. These time scales are chosen in order to allow a direct comparison with MAPI for which it is known that the important degradation effect become visible after one week, and have progressed very significantly after one month (comparative results for MAPI are presented in the Supplementary Information). Correlation of the response to these tests and controls allowed the effects of each of these factors to be isolated, as shown in **Table 3** and **4**. The set of environmental exposure conditions in the table was chosen to collectively reveal the individual effects of water vapour, air, O_2, UV and day lighting on the materials. Table 4 presents the logic table used to isolate each. Oxygen is a common factor in each of test numbers 2, 3 and 4, but the transformation for each is different, hence oxygen cannot be responsible for triggering the phase change. Similar logic was applied to

evaluate the effect of the other factors. The characterisation results are shown in **Figure 4** a-d.

It was found that significant changes to the material were caused only by exposure to water vapour (i.e. exposure to ambient air in the dark), with both exposure to ambient light in dry conditions, and short UV/O_3 exposure (in dry air) having no effect. Films affected by water vapour (in just a few hours or less, depending on the ambient relative humidity) showed a complete change of their XRD patterns and a shift in their optical absorption threshold from 1.92 to 2.85 eV, which accompanied the change from brown to yellow. Water vapour, independently from the presence or absence of light, was therefore identified as the principal cause of the phase transformation of the $CsPbI_2Br$.

In addition, long exposure to UV light in dry conditions was identified as a second, but less severe factor causing change to the films. Figure 4c,d show that for films exposed to a UV lamp for one month, there is broadening and displacement of the XRD peaks, and an accompanying reduction in optical absorption. Also, the films took on a mottled appearance with the development of dark yellow areas in the otherwise brown films (see Figure S4). Clearly this prolonged intense UV exposure promotes change from brown to yellow $CsPbI_2Br$, but more slowly than is caused by water vapour. Overall, 'degradation' caused by water vapour is the most rapid and important degradation route for this material and the exact nature of the change is explored in the next section.

In order to provide the reader with a comparison to the degradation of MAPI, which is now well known, the results of exposure of MAPI to the same degradation factors in like-for-like trials are provided in the Supplementary Information Figure S6 and S7 and Table S1. $CsPbI_2Br$ is susceptible to water vapour, whereas MAPI is more easily degraded by exposure to light in combination with oxygen. Overall, $CsPbI_2Br$ is affected by fewer degradation factors than is MAPI.

Degradation conditions					Characterisation			
Degradation test name	**Illumination**	**Containment**	**Atmosphere**	**Duration**	**Visual**	**XRD**	**Optical**	**Conclusion**
1. UV/N_2 glovebox	UV lamp	Glovebox	Dry N_2; < 10ppm H_2O	One week	Brown (unchanged)	Unchanged	Unchanged	Strong UV-rad for long time produces changes in structure
				One month	Brown with yellow spots	Changed (peaks shift)	Changed (E_g shifts)	
2. Dark in air	Dark	None	Air with ~40% RH	One week	Yellow/transparent	Completely changed	Changed (E_g shifts)	Humidity provokes changes in structure immediately
				One month	Yellow/transparent	Completely changed	Changed (E_g shifts)	
3. Desiccator ambient light	Lab lighting	Desiccator with silica gel	Dry air (RH ≤15%)	One week	Brown (unchanged)	Unchanged	Unchanged	Ambient light does not affect structure
				One month	Brown (unchanged)	Unchanged	Unchanged	
4. UV/O_3 air	UV lamp	Inside UV/ozone cleaner	Dry air with ozone	54 min	Brown (slightly discoloured)	Unchanged	Unchanged	UV + O_3 do not affect structure

Table 3. Summary of the degradation tests performed on $CsPbI_2Br$ and the results of XRD and optical characterisation. It was concluded that the most significant cause of transformation from the brown to the yellow phase was the presence of water vapour.

Test name	Factor tested					Result on $CsPbI_2Br$
	UV	**O_3**	**Water vapour**	**O_2**	**Room light**	
1. UV/N_2 glovebox	Yes	No	No	No	No	No change
2. Dark in air	No	No	Yes	Yes	No	Change from brown to yellow
3. Desiccator ambient light	No	No	No	Yes	Yes	No change
4. UV/O_3 air	Yes	Yes	Low	Yes	No	Slow degradation

Table 4. Logic table for the degradation experiments showing how the tests collectively reveal the importance of each individual degradation factor. Further details of each test are given in Table 3.

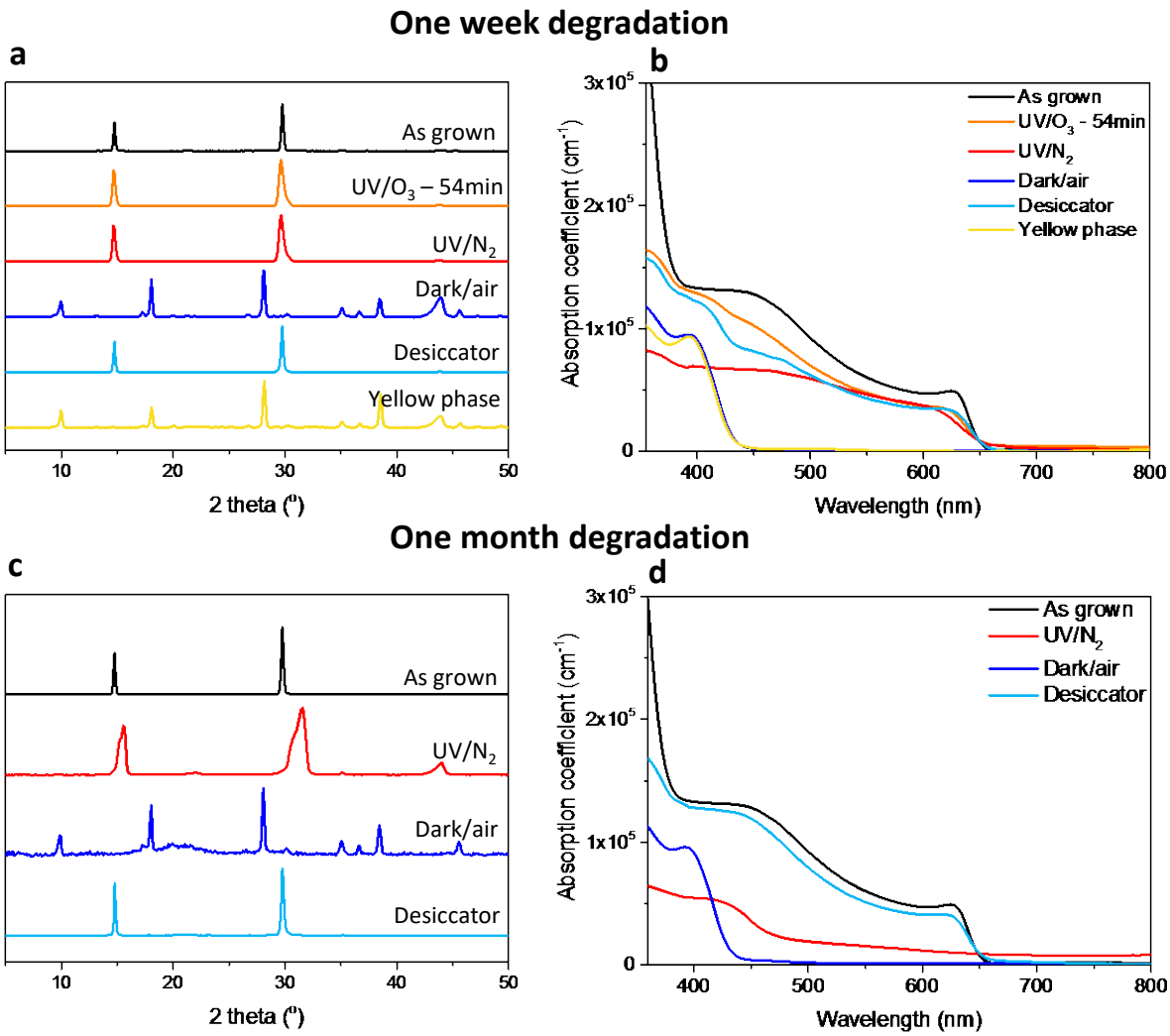

Figure 4. Response of $CsPbI_2Br$ to degradation factors: XRD and optical absorption data for films held under controlled conditions for one week (a,b) and one month (c,d) compared to as-grown samples. The effects of exposure in a UV/ozone cleaner for 54 mins are also included in panels a) and b).
One week in the dark under room air promoted complete change from the brown to the yellow phase, whereas one month's exposure to UV light under dry conditions was required to promote an incomplete change. Since the other conditions tested were all dry, water vapour was highlighted as the most important degradation medium for $CsPbI_2Br$ films.

Phase transformation mechanism and its reversibility

As the XRD pattern in Figure 4a,c shows that the crystal structure of the aged (yellow) form of $CsPbI_2Br$ does not correspond to any of its component salts (see Supplementary Information), it was suspected that the aged films comprise a new phase rather than a decomposition product. Indeed, it was found that the water vapour induced transformation from brown to yellow could be reversed by heating to 350°C on the hotplate under nitrogen, as shown in **Figure 5**a. This was confirmed by XRD (as shown in Figure 5b) and there was a

corresponding return to the lower optical band gap. Hence the material is considered to transform reversibly between the brown and yellow phases without degrading.

In order to investigate the role of water further we made sufficient quantities of bulk powder $CsPbI_2Br$ for physical investigations by dripping the halide precursor solution onto a glass plate at 350°C, as described in the Supplementary Information.

Firstly we conducted differential scanning calorimentry/thermo-gravimetric analysis (DSC-TGA) in order to check for possible phase transformations and weight loss. Figure 5c shows the results for both fresh and degraded powder samples. In the DSC trace for both samples the main feature is an exotherm at 463°C which corresponds to melting. There is also a very small exothermic DSC peak visible for the yellow, but not the brown sample at ~255°C – this may therefore represent the 'reverse' phase transition from the yellow to the brown phase. However, there is no peak in the DSC nor weight loss in the TGA that indicates any possible loss of water.

Secondly, we performed a proton nuclear magnetic resonance (^{1}H NMR) on samples of both fresh and aged powder of $CsPbI_2Br$ dissolved in deuterated DMSO (see Supplementary Information). The result, shown in Figure 5d,e shows the expected quintuplet of peaks from the solvent for both fresh and aged samples. However, while both samples show an identical small peak at 3.3 ppm which is the expected position for water, this is presumed to be an impurity in the solvent,[39] and is the same for both samples.

We therefore infer from the DSC-TGA and ^{1}H NMR that the aged yellow phase of $CsPbI_2Br$ does not contain water as a major component, but that nevertheless, water promotes the transformation from the brown to the yellow phase of $CsPbI_2Br$.

The most plausible explanation of the behaviour of the $CsPbI_2Br$ material explored above is in terms of the transformation between its low- and high-temperature phases. Its stable room temperature phase is yellow and has too high a bandgap for PV. It is the high temperature brown phase that is useful for PV, and this phase is metastable at room temperature.

During synthesis, if the material is processed at high temperatures, then it converts fully to the brown phase. Our DSC indicates the phase change takes place at 255°C (rather higher than the 195°C reported by Sharma *et al.*[25] in which there is a scatter of data points). In practice we found that 350°C was a workable processing temperature for the formation of fully uniform brown films having the cubic structure and able to give PV devices with relatively high *PCE*.

When stored under dry conditions the films were very stable and did not revert to the yellow phase. Indeed, in like for like tests, brown phase $CsPbI_2Br$ was more stable to a wide range of degradation test conditions

than was MAPI (see Supplementary Information, Figure S7). Hence the brown phase, although in principle metastable, is potentially of practical value for PV applications.

Since water vapour has been shown by this work to destabilise the brown phase of $CsPbI_2Br$ we have paid considerable attention to its role. In particular we wished to investigate the possibility that the yellow phase might be a hydrated phase rather than the true orthorhombic low temperature phase of anhydrous $CsPbI_2Br$. (A relevant analogy is from an important study conducted by Leguy *et al.*[1] of the effect of water on MAPI in which the hydrated phase $(CH_3NH_3)_4PbI_6{\cdot}2H_2O$ was identified). However our DSC and NMR experiments failed to show significant quantities of water in the yellow phase. Hence we ruled out the idea that the change from the brown to the yellow phase was as the result of absorption of water as a major component: the results support the hypothesis that the yellow and brown phases are indeed simply the low and high temperature phases of the compound $CsPbI_2Br$.

Nevertheless, water does play a role and is indeed necessary to induce the change from the brown phase to the yellow phase. Visual monitoring of brown-phase $CsPbI_2Br$ films reveals that they do not fade to yellow uniformly, but that the change starts at points, which grow into spots that eventually take over the whole film: moisture appears to induce the transformation starting at macroscopic nucleation sites. Overall our results support the hypothesis that water vapour acts to trigger reversion of the metastable high temperature phase to the stable low temperature one which is thermodynamically favoured. It may be speculated that water interacts with near-surface metal ions in the brown phase cubic $CsPbI_2Br$ in such a way as to destabilise the metastable crystal structure. In contrast, the reversibility of the films can be explained as a reverse phase transformation; it is likely that heating above the phase boundary at 255°C acts to simply transform the material back to its high temperature phase driving off any surface-absorbed water.

Considering the above, the phase transformation effects may be concluded to be simply caused by the material's passing over the low to high temperature phase boundary. Synthesis at a sufficiently high temperature creates the (metastable) brown cubic phase of $CsPbI_2Br$, which is stable under dry conditions. Exposure to water vapour triggers transformation to the yellow room temperature phase, but re-heating above the phase boundary reverses this change.

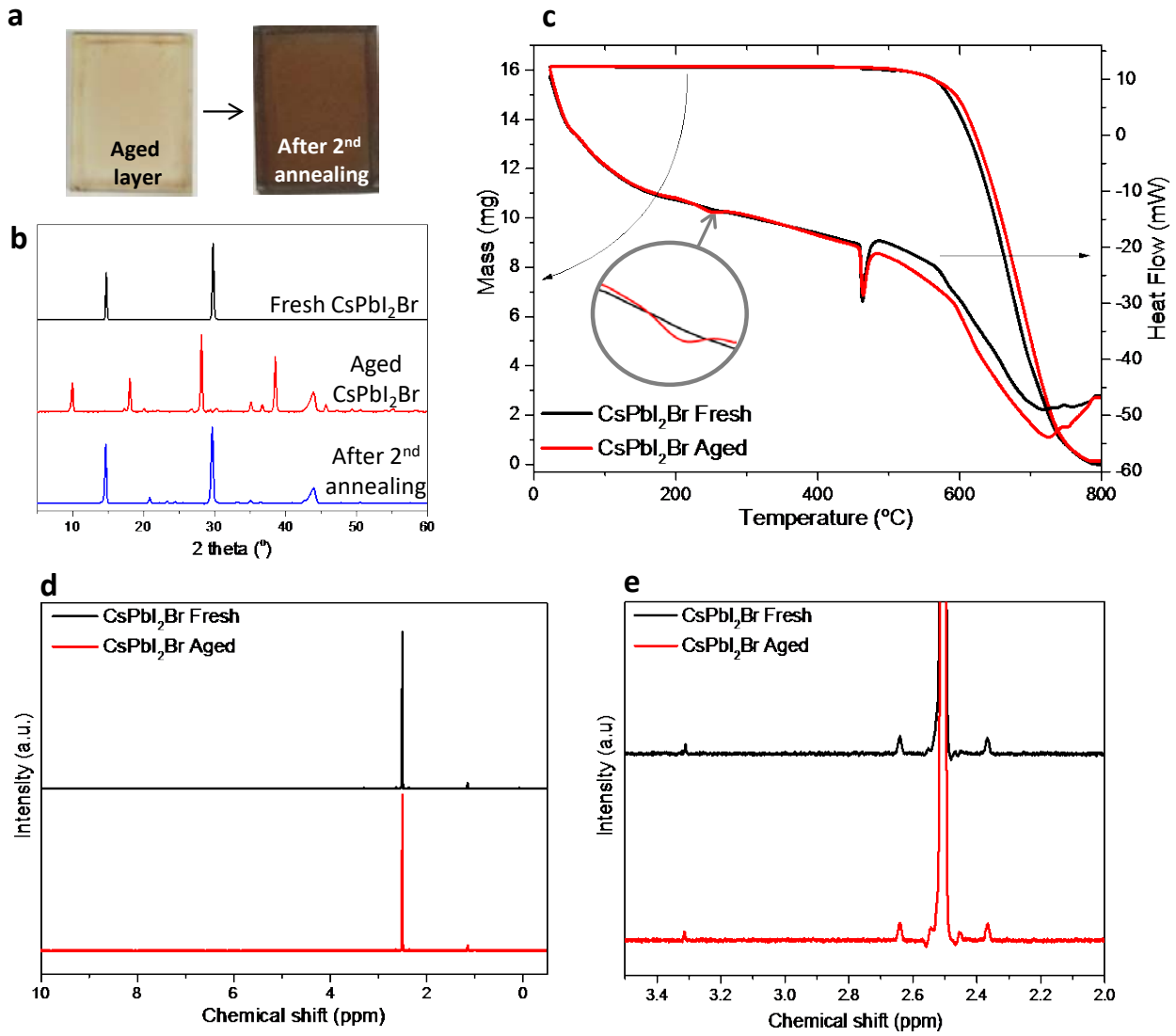

Figure 5. Physical investigation of the effects of water vapour on $CsPbI_2Br$. (a) Photographs of an aged film before (yellow) and after (brown) recovery by heating at 350°C (2nd anneal). (b) XRD pattern of films demonstrating that for aged films the original cubic crystal structure is re-established after annealing. (c) DSC-TGA of both fresh and aged powder samples. There is a melting peak at 463°C for both samples and a small exotherm at 255°C for the aged sample. (d,e) ^{1}H NMR of fresh and degraded samples in d^6-DMSO. These show only peaks from the solvent. We conclude that the transformation from the brown to the yellow phase does not cause water to be included in the structure as a major component, and is reversible by heating.

Device stability

We now describe the effects of the $CsPbI_2Br$ phase change on the performance of devices and its reversibility. Table 2 and **Figure 6** compare the solar cell performances of both as-grown devices and those aged in air for 24 hours. Figure 6a shows that the performance degradation is via a collapse of the *J-V* curve with a corresponding crash in efficiency from 6.46% to 0.08%. Similar efficiency losses, also driven by a collapse in the current, were observed for cells having absorbers made at all temperatures in the range 150-350°C

(Figure 6b and Table 2). This loss of current is a direct consequence of the phase change from the absorbing brown phase (E_g = 1.82 eV) to the more transparent yellow phase (E_g = 2.25 eV) as shown in Figure 3. Remarkably, the V_{OC} maintains its > 75% of its value after degradation (Figure 6c), and this is likely to be a consequence of there being favourable band line ups for both of the phases.

Recovery of device performance

We investigated the influence of reversing the phase change on the performance of devices. This was done by preparing devices from films of $CsPbI_2Br$ that were either a) freshly prepared in the brown perovskite phase form, or b) had been allowed to transform to the yellow phase in humid air (aged devices) - and then had been recovered by annealing at 350°C. Both were finished with Spiro-OMeTAD and Au contacts to form complete devices. This protocol allowed us to isolate the effects of annealing of the $CsPbI_2Br$ from any possible unintended degradation of the Spiro-OMeTAD. Sets of 16 devices of each type were prepared in each test and this was repeated four times. Typical *J*–*V* curves for 'as-grown', 'degraded' and 'recovered' devices are shown in Figure 6d. In all cases the recovered devices showed greater efficiencies than the as-grown ones, with the improvement in performance being up to 115% for individual devices. The average values were: as-grown: *PCE* = 5.42%, V_{OC} = 1.00 V, J_{SC} = 9.80 mA.cm^{-2} and *FF* = 55.6%; recovered: *PCE* = 5.42%, V_{OC} = 1.00 V, J_{SC} = 9.50 mA.cm^{-2} and *FF* = 56.1 %. From this, the performance increase is seen to be from a small increase in *FF* and this implies that the phase change is associated with an improvement in the materials quality, e.g. from a reorganisation of point or extended defects upon annealing.

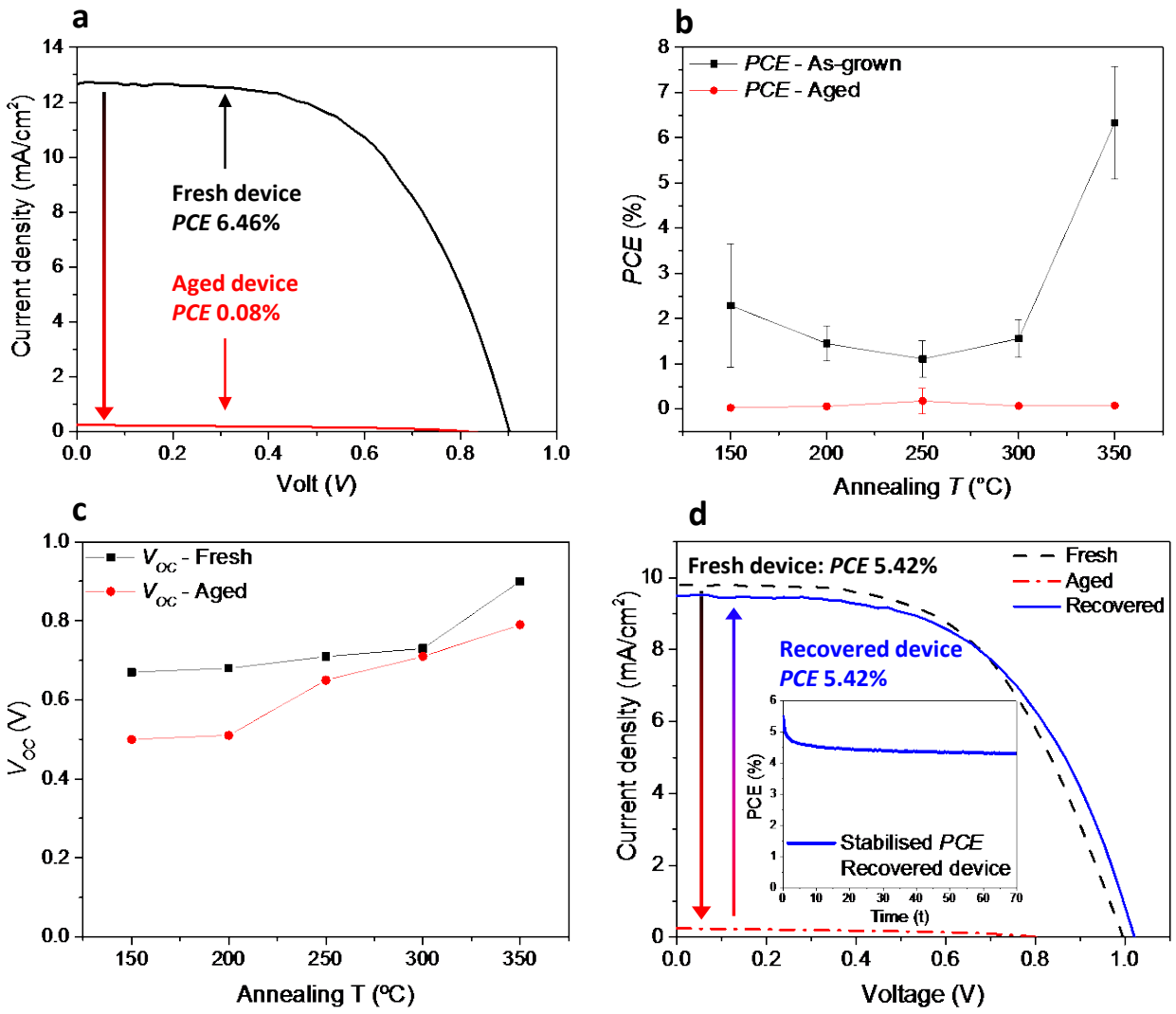

Figure 6. $CsPbI_2Br$ device ageing and recovery. (a) *J-V* curves from as-grown and aged devices showing that the performance loss is due to low current generation; (b) dependence of the device performance and its degradation on the preparation temperature of the $CsPbI_2Br$ absorber; (c) comparison of the open circuit-voltage of devices before and after ageing showing that ageing has little effect on V_{OC}; (d) *J-V* curve of as-grown, aged and recovered devices showing that re-annealing promotes complete recovery of the device performance from its degraded state.

Conclusion

In summary, the mixed caesium lead halide perovskite $CsPbI_2Br$ is of interest since its lower band gap is more suited to solar energy conversion than $CsPbBr_3$, and it is more stable than the pure tri-iodide analogue. We have extended what is known about $CsPbI_2Br$ by reporting the first degradation studies in dry air, oxygen and visible light. This has demonstrated that $CsPbI_2Br$ rather than degrading into its original components, transforms from its low band gap (E_g = 1.92 eV) brown cubic phase to a higher band gap (E_g = 2.85 eV) yellow orthorhombic form in the presence of water vapour. We have also shown that the yellow phase does not contain significant fractions of water even though its crystal structure differs from that of the brown phase.

While transformation of $CsPbI_2Br$ takes place in open lab conditions, we have shown that unlike MAPI it transforms to a new phase (its stable room temperature orthorhombic phase) rather than degrading irreversibly to its component salts. Moreover, for $CsPbI_2Br$ heating at 350°C reverses the transformation and recovers the original crystal structure. It was also shown that PV devices made from $CsPbI_2Br$ films that had been transformed and then re-generated by annealing had up to 115% of the efficiency of those made from fresh films i.e. the process of transformation and recovery increases the PV performance. Nevertheless, the as-made devices did lose performance under room conditions, but remarkably even though their *PCE* performances dropped to < 0.1%, their open circuit voltages remained high (75% of the original V_{OC}). The efficiency loss was therefore attributed to the widening of the band gap upon transformation from the brown to the yellow phase of $CsPbI_2Br$. The highest efficiency obtained in this work for a glass/ITO/c-TiO_2/$CsPbI_2Br$/Spiro-OMeTAD/Au PV device was 9.08% which is comparable to the highest reported value (9.84%) to within the accuracy of routine laboratory measurements. We conclude that encapsulation of $CsPbI_2Br$ to exclude water vapour should be sufficient to stabilise the cubic brown phase, making the material of interest for use in practical PV devices.

Acknowledgments

This research has been funded by EPSRC Centre for Doctoral Training in New and Sustainable Photovoltaics CDT-PV, EP/L01551X/1. The authors would also like to thank Prof. A. J. Pal, IACS Kolkata for the helpful discussions and assistance from his laboratory.

References

(1) Leguy, A. M. A.; Hu, Y.; Campoy-Quiles, M.; Alonso, M. I.; Weber, O. J.; Azarhoosh, P.; van Schilfgaarde, M.; Weller, M. T.; Bein, T.; Nelson, J.; Docampo, P.; Barnes, P. R. F. Reversible Hydration of $CH_3NH_3PbI_3$ in Films, Single Crystals, and Solar Cells. *Chem. Mater.* **2015**, *27* (9), 3397–3407.

(2) Christians, J. A.; Miranda Herrera, P. A.; Kamat, P. V. Transformation of the Excited State and Photovoltaic Efficiency of $CH_3NH_3PbI_3$ Perovskite upon Controlled Exposure to Humidified Air. *J. Am. Chem. Soc.* **2015**, *137* (4), 1530–1538.

(3) Mosconi, E.; Azpiroz, J. M.; De Angelis, F. *Ab Initio* Molecular Dynamics Simulations of Methylammonium Lead Iodide Perovskite Degradation by Water. *Chem. Mater.* **2015**, *27* (13), 4885–4892.

(4) Correa-Baena, J.-P.; Abate, A.; Saliba, M.; Tress, W.; Jesper Jacobsson, T.; Grätzel, M.; Hagfeldt, A. The Rapid Evolution of Highly Efficient Perovskite Solar Cells. *Energy Environ. Sci.* **2017**, *10* (3), 710–727.

(5) Aristidou, N.; Sanchez-Molina, I.; Chotchuangchutchaval, T.; Brown, M.; Martinez, L.; Rath, T.; Haque, S. A. The Role of Oxygen in the Degradation of Methylammonium Lead Trihalide Perovskite Photoactive Layers. *Angew. Chem. Int. Ed. Engl.* **2015**, *54* (28), 8208–8212.

(6) Aristidou, N.; Eames, C.; Sanchez-Molina, I.; Bu, X.; Kosco, J.; Islam, M. S.; Haque, S. A. Fast Oxygen Diffusion and Iodide Defects Mediate Oxygen-Induced Degradation of Perovskite Solar Cells. *Nat. Commun.* **2017**, *8*, 15218–15227.

(7) Bryant, D.; Aristidou, N.; Pont, S.; Sanchez-Molina, I.; Chotchunangatchaval, T.; Wheeler, S.; Durrant, J. R.; Haque, S. A. Light and Oxygen Induced Degradation Limits the Operational Stability of Methylammonium Lead Triiodide Perovskite Solar Cells. *Energy Environ. Sci.* **2016**, *9* (5), 1655–1660.

(8) Device Stability of Perovskite Solar Cells – A Review. *Renew. Sustain. Energy Rev.* **2017**, *77*, 131–146.

(9) Sanchez, R. S.; Gonzalez-Pedro, V.; Lee, J.-W.; Park, N.-G.; Kang, Y. S.; Mora-Sero, I.; Bisquert, J. Slow Dynamic Processes in Lead Halide Perovskite Solar Cells. Characteristic Times and Hysteresis. *J. Phys. Chem. Lett.* **2014**, *5* (13), 2357–2363.

(10) Kim, H.-S.; Park, N.-G. Parameters Affecting I – V Hysteresis of $CH_3NH_3PbI_3$ Perovskite Solar Cells: Effects of Perovskite Crystal Size and Mesoporous TiO_2 Layer. *J. Phys. Chem. Lett.* **2014**, *5* (17), 2927–2934.

(11) Butler, K. T.; Frost, J. M.; Walsh, A. Band Alignment of the Hybrid Halide Perovskites $CH_3NH_3PbCl_3$, $CH_3NH_3PbBr_3$ and $CH_3NH_3PbI_3$. *Mater. Horiz.* **2015**, *2* (2), 228–231.

(12) Im, J.-H.; Chung, J.; Kim, S.-J.; Park, N.-G. Synthesis, Structure, and Photovoltaic Property of a Nanocrystalline 2H Perovskite-Type Novel Sensitizer $(CH_3CH_2NH_3)PbI_3$. *Nanoscale Res. Lett.* **2012**, *7* (1), 353–360.

(13) Gao, P.; Grätzel, M.; Nazeeruddin, M. K. Organohalide Lead Perovskites for Photovoltaic Applications. *Energy Environ. Sci.* **2014**, *7* (8), 2448–2463.

(14) Pisanu, A.; Ferrara, C.; Quadrelli, P.; Guizzetti, G.; Patrini, M.; Milanese, C.; Tealdi, C.; Malavasi, L. The $FA_{1-x}MA_xPbI_3$ System: Correlations among Stoichiometry Control, Crystal Structure, Optical Properties, and Phase Stability. *J. Phys. Chem. C* **2017**, *121* (16), 8746–8751.

(15) Abate, A.; Saliba, M.; Hollman, D. J.; Stranks, S. D.; Wojciechowski, K.; Avolio, R.; Grancini, G.; Petrozza, A.; Snaith, H. J. Supramolecular Halogen Bond Passivation of Organic–Inorganic Halide Perovskite Solar Cells. *Nano Lett.* **2014**, *14* (6), 3247–3254.

(16) Saliba, M.; Matsui, T.; Seo, J.-Y.; Domanski, K.; Correa-Baena, J.-P.; Nazeeruddin, M. K.; Zakeeruddin, S. M.; Tress, W.; Abate, A.; Hagfeldt, A.; Grätzel, M. Cesium-Containing Triple Cation Perovskite Solar Cells: Improved Stability, Reproducibility and High Efficiency. *Energy Environ. Sci.* **2016**, *9* (6), 1989–1997.

(17) Li, X.; Ibrahim Dar, M.; Yi, C.; Luo, J.; Tschumi, M.; Zakeeruddin, S. M.; Nazeeruddin, M. K.; Han, H.; Grätzel, M. Improved Performance and Stability of Perovskite Solar Cells by Crystal Crosslinking with Alkylphosphonic Acid ω-Ammonium Chlorides. *Nat. Chem.* **2015**, *7* (9), 703–711.

(18) Grancini, G.; Roldán-Carmona, C.; Zimmermann, I.; Mosconi, E.; Lee, X.; Martineau, D.; Narbey, S.; Oswald, F.; De Angelis, F.; Graetzel, M.; Nazeeruddin, M. K. One-Year Stable Perovskite Solar Cells by 2D/3D Interface Engineering. *Nat. Commun.* **2017**, *8*, 15684.

(19) Noel, N. K.; Abate, A.; Stranks, S. D.; Parrott, E. S.; Burlakov, V. M.; Goriely, A.; Snaith, H. J. Enhanced Photoluminescence and Solar Cell Performance via Lewis Base Passivation of Organic–Inorganic Lead Halide Perovskites. *ACS Nano* **2014**, *8* (10), 9815–9821.

(20) Grätzel, M. The Rise of Highly Efficient and Stable Perovskite Solar Cells. *Acc. Chem. Res.* **2017**, *50* (3), 487–491.

(21) Leijtens, T.; Bush, K.; Cheacharoen, R.; Beal, R.; Bowring, A.; McGehee, M. D. Towards Enabling Stable Lead Halide Perovskite Solar Cells; Interplay between Structural, Environmental, and Thermal Stability. *J. Mater. Chem. A* **2017**, *5* (23), 11483–11500.

(22) Zhu, X.; Yang, D.; Yang, R.; Yang, B.; Yang, Z.; Ren, X.; Zhang, J.; Niu, J.; Feng, J.; Liu, S. (Frank). Superior Stability for Perovskite Solar Cells with 20% Efficiency Using Vacuum Co-Evaporation. *Nanoscale* **2017**, *9* (34), 12316–12323.

(23) Eperon, G. E.; Stranks, S. D.; Menelaou, C.; Johnston, M. B.; Herz, L. M.; Snaith, H. J. Formamidinium Lead Trihalide: A Broadly Tunable Perovskite for Efficient Planar Heterojunction Solar Cells. *Energy Environ. Sci.* **2014**, *7* (3), 982–988.

(24) Møller, C. K. Crystal Structure and Photoconductivity of Cæsium Plumbohalides. *Nature* **1958**, *182* (4647), 1436–1436.

(25) Sharma, S.; Weiden, N.; Weiss, A. Phase Diagrams of Quasibinary Systems of the Type: ABX_3 - $A'BX_3$; ABX_3 - $AB'X_3$, and ABX_3 — ABX_3; X = Halogen Crystal Structure / Phase Diagrams / Phase Transitions / X-Ray Diffraction. **1992**, *175*, 63–80.

(26) Green, M. A.; Ho-Baillie, A.; Snaith, H. J. The Emergence of Perovskite Solar Cells. *Nat. Photonics* **2014**, *8* (7), 506–514.

(27) Sutton, R. J.; Eperon, G. E.; Miranda, L.; Parrott, E. S.; Kamino, B. A.; Patel, J. B.; Hörantner, M. T.; Johnston, M. B.; Haghighirad, A. A.; Moore, D. T.; Snaith, H. J. Bandgap-Tunable Cesium Lead Halide Perovskites with High Thermal Stability for Efficient Solar Cells. *Adv. Energy Mater.* **2016**, *6*, 150258–150464.

(28) Beal, R. E.; Slotcavage, D. J.; Leijtens, T.; Bowring, A. R.; Belisle, R. A.; Nguyen, W. H.; Burkhard, G.; Hoke, E. T.; McGehee, M. D. Cesium Lead Halide Perovskites with Improved Stability for Tandem Solar Cells. *J. Phys. Chem. Lett.* **2016**, *7*, 746–751.

(29) Eperon, G. E.; Paternò, G. M.; Sutton, R. J.; Zampetti, A.; Haghighirad, A. A.; Cacialli, F.; Snaith, H. J. Inorganic Caesium Lead Iodide Perovskite Solar Cells. *J. Mater. Chem. A* **2015**, *3* (39), 19688–19695.

(30) Møller, C. K. The Structure of Perovskite-like Cæsium Plumbo Trihalides. *Mat. Fys. Medd. Dan. Vid. Selsk* **1959**, *32* (2).

(31) Brasseur, H.; Pauling, L. The Crystal Structure of Ammonium Cadmium Chloride, NH_4CdCl_3. *J. Am. Chem. Soc.* **1938**, *60* (12), 2886–2890.

(32) Dastidar, S.; Egger, D. A.; Tan, L. Z.; Cromer, S. B.; Dillon, A. D.; Liu, S.; Kronik, L.; Rappe, A. M.; Fafarman, A. T. High Chloride Doping Levels Stabilize the Perovskite Phase of Cesium Lead Iodide. *Nano Lett.* **2016**, *16* (6), 3563–3570.

(33) Kulbak, M.; Cahen, D.; Hodes, G. How Important Is the Organic Part of Lead Halide Perovskite Photovoltaic Cells? Efficient $CsPbBr_3$ Cells. *J. Phys. Chem. Lett.* **2015**, *6* (13), 2452–2456.

(34) Song, J.; Li, J.; Li, X.; Xu, L.; Dong, Y.; Zeng, H. Quantum Dot Light-Emitting Diodes Based on Inorganic Perovskite Cesium Lead Halides ($CsPbX_3$). *Adv. Mater.* **2015**, *27* (44), 7162–7167.

(35) Bi, D.; Tress, W.; Dar, M. I.; Gao, P.; Luo, J.; Renevier, C.; Schenk, K.; Abate, A.; Giordano, F.; Correa Baena, J.-P.; Decoppet, J.-D.; Zakeeruddin, S. M.; Nazeeruddin, M. K.; Grätzel, M.; Hagfeldt, A. Efficient Luminescent Solar Cells Based on Tailored Mixed-Cation Perovskites. *Sci. Adv.* **2016**, *2* (1), e1501170–e1501170.

(36) Shockley, W.; Queisser, H. J. Detailed Balance Limit of Efficiency of P-N Junction Solar Cells. *J. Appl. Phys.* **1961**, *32* (3), 510–519.

(37) Stoumpos, C. C.; Malliakas, C. D.; Peters, J. A.; Liu, Z.; Sebastian, M.; Im, J.; Chasapis, T. C.; Wibowo, A. C.; Chung, D. Y.; Freeman, A. J.; Wessels, B. W.; Kanatzidis, M. G. Crystal Growth of the Perovskite Semiconductor $CsPbBr_3$: A New Material for High-Energy Radiation Detection. *Cryst. Growth Des.* **2013**, *13* (7), 2722–2727.

(38) Nikl, M.; Nitsch, K.; Chval, J.; Somma, F.; Phani, A. R.; Santucci, S.; Giampaolo, C.; Fabeni, P.; Pazzi, G. P.; Feng, X. Q. Optical and Structural Properties of Ternary Nanoaggregates in CsI-PbI_2 Co-Evaporated Thin Films. *J. Phys. Condens. Matter* **2000**, *12* (8), 1939–1946.

(39) Gottlieb, H. E.; Kotlyar, V.; Nudelman, A. NMR Chemical Shifts of Common Laboratory Solvents as Trace Impurities. *J. Org. Chem.* **1997**, *62* (21), 7512–7515.

Supporting Information. The Supporting Information is available free of charge on the ACS Publications website at DOI:

Experimental details, materials and device fabrication, testing and degradation conditions, EQE analysis, $CsPbI_2Br$ transmittance and reflectance spectra after different environmental conditions and related pictures of the samples, XRD on $CsPbI_2Br$ yellow phase and possible associated patterns, degradation experiments on MAPI with pictures, transmittance, reflectance and absorption coefficient spectra and related table.

TOC graphics